

Deep Learning to Assess Glaucoma Risk and Associated Features in Fundus Images

Sonia Phene, BS^{1*}
R. Carter Dunn, MS, MBA^{1*}
Naama Hammel, MD^{1*}
Yun Liu, PhD¹
Jonathan Krause, PhD¹
Naho Kitade, BA¹
Mike Schaeckermann, BS¹
Rory Sayres, PhD¹
Derek J. Wu, BS¹
Ashish Bora, MS¹
Christopher Semturs, MS¹
Anita Misra, BTech¹
Abigail E. Huang, MD¹
Arielle Spitze, MD^{2,3}
Felipe A. Medeiros, MD, PhD⁴
April Y. Maa, MD^{5,6}
Monica Gandhi, MD⁷
Greg S. Corrado, PhD¹
Lily Peng, MD, PhD^{1**}
Dale R. Webster, PhD^{1**}

*Equal contribution

**Equal contribution

Affiliations:

¹Google AI Healthcare, Google LLC, Mountain View, CA, USA

²Virginia Ophthalmology Associates, Norfolk, VA, USA

³Department of Ophthalmology, Eastern Virginia Medical School, Norfolk, VA

⁴Department of Ophthalmology, Duke University, Durham, NC, USA

⁵Department of Ophthalmology, Emory University School of Medicine, Atlanta, GA, USA

⁶Ophthalmology Section, Atlanta Veterans Affairs Medical Center, Atlanta, GA, USA

⁷Dr. Shroff's Charity Eye Hospital, New Delhi, India

Corresponding Author: Naama Hammel, MD

Google AI Healthcare, Google LLC

1600 Amphitheatre Pkwy, Mountain View, CA 94043

nhammel@google.com

Abstract

Purpose: Develop and validate a deep learning (DL) algorithm that predicts referable glaucoma risk and detects glaucomatous optic nerve head (ONH) features from color fundus images, determine the relative importance of these features in the referral assessment by glaucoma specialists, and compare the performance of the algorithm with eye-care providers and a screening program.

Design: Development and validation of a DL algorithm.

Participants: Fundus images from screening programs, studies, and clinics.

Methods: A DL algorithm was trained using a retrospective dataset of 58,033 images, assessed for gradability, glaucomatous ONH features, and referable glaucoma risk by a panel of 41 graders. The resultant algorithm was validated using 2 separate datasets. Validation dataset “A” (1,205 images, 1 image/patient; 19% referable) consisted of images adjudicated by panels of fellowship-trained glaucoma specialists, and validation dataset “B” (17,593 images from 9,643 patients; 9.2% referable) consisted of images from the Atlanta Veterans Affairs (VA) Eye Clinic diabetic teleretinal screening program using clinical referral decisions as the reference standard.

Main outcome measures: The DL algorithm was evaluated using area under the receiver operating characteristic curve (AUC), sensitivity, and specificity for detecting referable glaucoma risk and glaucomatous ONH features.

Results: The DL algorithm had an AUC of 0.940 (95%CI, 0.922-0.955) in validation dataset “A” and 0.858 (95% CI, 0.836-0.878) in validation dataset “B” for referable glaucoma risk. Algorithm AUCs ranged between 0.608-0.977 for glaucomatous ONH features. The algorithm was significantly more sensitive than 6 of 10 graders, including 2 of 3 glaucoma specialists, with comparable or higher specificity relative to all graders. The presence of vertical cup-to-disc ratio

≥ 0.7 , neuroretinal rim notching, retinal nerve fiber layer (RNFL) defect, or bared circumlinear vessels contributed most to referable glaucoma risk assessment by both glaucoma specialists and the algorithm.

Conclusions: A DL algorithm trained on fundus images alone can detect referable glaucoma risk with higher sensitivity and comparable specificity to eye care providers. The most significant ONH features used for referable glaucoma risk assessment were similar between glaucoma specialists and the algorithm.

Key words: Glaucoma, Deep Learning, Glaucomatous ONH features, Screening, Teleophthalmology

Introduction

Glaucoma, the “silent thief of sight”, is the leading cause of preventable, irreversible blindness world-wide.^{1,2} Glaucoma currently affects about 70 million individuals, and is projected to affect about 112 million individuals in 2040.² The disease can remain asymptomatic until severe, and an estimated 50%-90% of people with glaucoma remain undiagnosed.³⁻⁵ Thus, glaucoma screening is recommended for early detection and treatment.^{6,7} However, this currently requires a clinical exam combined with quantitative functional and structural measurements, accessible only to a small percentage of the world’s population. A cost-effective tool that can detect glaucoma could expand access to a much larger patient population. Such a tool is currently unavailable.⁸

Retinal fundus photography is a well-established diagnostic tool for eye diseases, enabling fundus images to be evaluated for the presence of retinal and optic nerve head (ONH) pathologies.^{9,10,8} Glaucoma, characterized by progressive degeneration of retinal ganglion cells and loss of their axons, results in characteristic changes in the appearance of the ONH and retinal nerve fiber layer (RNFL).¹¹ These changes can be detected in fundus images¹² and are the most important aspects of glaucoma diagnosis.¹³

Physical features that have been associated with glaucomatous optic neuropathy (GON) include neuroretinal rim thinning and/or notching, increased cup-to-disc ratio (CDR), CDR asymmetry, excavation of the cup, RNFL thinning, disc hemorrhages, parapapillary atrophy (PPA), laminar dots, nasalization of central ONH vessels, and barring of circumlinear vessels.^{14,15} However, several of the features listed may appear in otherwise healthy optic nerves,^{16,17} may result from non-glaucomatous pathology,^{18,19,20} or are poorly defined in the literature.²¹ The relative importance of these features for the diagnosis of glaucoma has not been validated, and

practitioners may weigh features differently, often focusing on increased CDR, neuroretinal rim thinning and notching, disc hemorrhages, and RNFL defects.²²

Deep learning (DL)²³ has been applied to produce highly accurate algorithms that can detect eye conditions such as diabetic retinopathy (DR) with accuracy comparable to human experts.^{24–26} The use of this technology may aid screening efforts, and recent work demonstrates value in assisting ophthalmologists.²⁷

DL algorithms have also been developed for other diseases, including glaucoma.^{26,28–31} However, the diagnosis of glaucoma poses several challenges that distinguish it from conditions such as DR. While DR has well-established clinical guidelines for diagnosis from fundus images, the diagnosis of glaucoma consists of the compilation of clinical exam data with functional and structural testing. There is no single agreed-upon set of guidelines for glaucoma detection from fundus images.³² Teleretinal screening programs have worked around these limitations by focusing on subsets of the potential diagnostic features present in fundus images. However, these criteria vary between programs and the relationship of the individual features to overall glaucoma assessment is not well characterized. This strongly limits the clinical value of these diagnoses, and correspondingly limits the values of DL algorithms developed around these heuristics.

The present work aims to extend the utility of DL algorithms, by explicitly bridging the gap between individual diagnostic features present in fundus imagery and overall glaucoma risk assessment by experts. We develop a model that is trained on both individual pathologies, as well as overall glaucoma referability. We ask: Can we develop a DL algorithm that performs at or above expert level in overall glaucoma suspect diagnosis? What is the relationship between individual features and overall glaucoma risk assessment for glaucoma experts? Do DL algorithms learn a similar relationship?

Methods

Datasets

Development datasets

The development datasets for this study consisted of fundus images obtained from multiple sources: EyePACS,³³ Inoveon,³⁴ and the Age Related Eye Disease Study (AREDS)³⁵ in the United States, three eye hospitals in India (Aravind Eye Hospital, Sankara Nethralaya, and Narayana Nethralaya), and the UK BioBank.³⁶

Validation datasets

Two datasets were used for validation. Validation dataset A was composed of a random subset of color fundus images from EyePACS, Inoveon, UK BioBank, AREDS, and Sankara Nethralaya. Validation dataset B was composed of macula-centered color fundus images from the Atlanta VA Eye Clinic diabetic teleretinal screening program.

All images were de-identified according to HIPAA Safe Harbor prior to transfer to the study investigators. Ethics review and Institutional Review Board approval was obtained by each participating institution. From each source, only one image from a given patient was used in the final analysis, and each image appeared only in either the development or validation sets.

Development Dataset Grading

Gradability

Graders assessed every image for gradability for each ONH feature and for referable glaucoma risk. If graders selected “ungradable” for a particular feature or referable glaucoma risk, then no grade was collected for that question.

Feature level grading

The American Academy of Ophthalmology's Primary Open-Angle Glaucoma Suspect Preferred Practice Patterns (PPP) provide a list of features that may indicate glaucomatous optic neuropathy: vertical elongation of the optic cup, excavation of the cup, thinning of the RNFL, notching of the neuroretinal rim, thinning of the inferior and/or superior neuroretinal rim, disc hemorrhage, parapapillary atrophy, nasalization of central ONH vessels, barring of the circumlinear vessel, and absence of neuroretinal rim pallor. Additionally, the finding of a laminar dot sign (visible lamina cribrosa fenestrations in the cup) is viewed by some clinicians as a sign of glaucomatous damage to the ONH.^{37,38} Violation of the ISNT (Inferior > Superior > Nasal > Temporal) neuroretinal rim area rule is viewed by some clinicians as a sign of glaucomatous rim loss. ISNT rule variants, focusing on the Inferior, superior and temporal quadrants have also been validated.³⁹ To enable systematic training of graders, we aggregated these features (**Table S1**), developed grading guidelines for each, and iterated on the guidelines with a panel of three fellowship-trained glaucoma specialists to increase inter-rater agreement.

Glaucoma risk grading

In addition to these features, we also developed guidelines for a four-point glaucoma risk assessment (as shown in **Table S1**) where the “high-risk glaucoma suspect” or “likely glaucoma” levels were considered referable. Graders were asked to provide an overall glaucoma risk grade after evaluating the image for each of the features on the list.

Graders

A total of 41 graders (13 fellowship-trained glaucoma specialists, 25 ophthalmologists, and 3 optometrists) were trained on the grading guidelines and were required to pass a certification test before being allowed to grade the development or validation A datasets.

Development of the Algorithm

Data preprocessing is detailed in the Supplement. Using this data, a deep convolutional neural network with the Inception-v3 architecture⁴⁰ was developed and trained in TensorFlow.⁴¹ Since our network had a large number of parameters (22 million), early stopping⁴² was used to terminate training before convergence. To speed up training, the network was initialized using parameters from a network pre-trained to classify objects in the ImageNet dataset⁴³. This procedure is similar to that previously described by Krause et al.²⁵

The development datasets consisted of two disjoint subsets: training and tuning. The training set of 58,033 images was used to optimize the network parameters. This dataset was enriched for referable glaucoma images using active learning,⁴⁴ a machine learning technique, to preferentially increase the number of relevant examples. The tuning set of 1,508 images was independently graded by three glaucoma specialists and was used to determine thresholds for three operating points for the algorithm: high sensitivity, high specificity, and a balanced sensitivity and specificity point (see Supplement for details). The tuning dataset and validation dataset “A” (described next) were randomly chosen from a pool that was also enriched, but using preliminary “screening” reviews by a separate panel of graders for images suspicious for glaucoma.

An ensemble of 10 networks⁴⁵ were trained on the same development set, and the outputs were averaged to yield the final prediction.

Clinical Validation Datasets

Two datasets were used for validation. For validation dataset A (1,205 images), the reference standard was determined by a rotating panel of 3 fellowship-trained glaucoma specialists (from a cohort of 12). Each image was first independently graded by each glaucoma specialist in the panel (“round 1”). For images where graders had disagreements, the same 3 glaucoma specialists (in a random order) reviewed the image a second time (“round 2”), this

time with access to the annotations and comments from round 1 and previous graders in round 2. Grader identities were anonymized throughout the grading process. Each image was reviewed a maximum of 6 times (2 from each grader), or fewer if consensus was reached before the 6th review. 49.3% (594 images) were fully adjudicated on all features and referable glaucoma risk by the completion of round 2.

For images unresolved after round 2, the reference standard for gradability, each ONH feature, and referable glaucoma risk was determined by the median of the 3 grades in round 2. The median corresponds to the majority vote if at least 2 graders agreed, and the “intermediate” grade if all 3 disagreed. This method was determined to closely approximate the full adjudication process described in Krause et al.²⁵ based on a comparison of multiple methods over 100 images described in **Table S2** and **S3**. Images for which the final grade was “ungradable” were excluded from further analysis.

For further evaluation on an independent population, the algorithm was also applied to a second validation dataset (validation dataset “B”, 17,593 images from 9,643 patients), composed of macula-centered color fundus images from the Atlanta VA Eye Clinic diabetic teleretinal screening program. Glaucoma-related International Classification of Diseases (ICD) codes and “optic nerve head” referral codes recorded in the patient’s medical history at any point in time prior to the capture of the image or up to 1 year after the image was taken were used as reference standard for this dataset. The specific codes used were ICD-9-CM codes for glaucoma (category 365) and ICD-10-CM codes for glaucoma (category H40). When a patient had an optic nerve head referral code on a particular visit, the image from that visit was chosen. When a patient with a glaucoma ICD code had multiple visits, the visit closest to the recorded date of the glaucoma-related ICD code was chosen.

Evaluating the Algorithm

The algorithm's performance was evaluated on the two validation datasets. The prediction for referable glaucoma risk was a continuous number between 0 and 1, corresponding to the predicted likelihood of that condition being present in the image. Receiver operating characteristic (ROC) curves were plotted by varying the operating threshold. To compare the performance of the algorithm with graders, a subset of 411 images from validation dataset A was graded by 10 graders (3 fellowship-trained glaucoma specialists, 4 ophthalmologists, and 3 optometrists). None of these graders participated in creating the reference standard for those images. For validation dataset B, for each eye of each patient, the classifier for referable glaucoma generated a continuous number between 0 and 1, corresponding to the probability of that condition being present in the corresponding image, and the maximum was taken across both eyes to get the final prediction.

Evaluating ONH feature importance

In order to assess which ONH features were weighed the most in grading for referable glaucoma risk, a multivariable logistic regression analysis was run to compute the odds ratio for each feature on overall referable glaucoma risk. Five logistic regression analyses were run on three datasets: the training dataset, the tuning dataset, and validation dataset "A". For validation dataset A, analyses were run using the reference standard, the round 1 median (see Clinical Validation Datasets section above), and the algorithm predictions.

Statistical Analysis

To compute the confidence intervals (CIs) for the algorithm's AUC, we used a non-parametric bootstrap procedure⁴⁶ with 2,000 samples. CIs for sensitivities and specificities were calculated using the exact Clopper-Pearson interval.⁴⁷ To compare the algorithm's performance (sensitivity and specificity) to graders, we used the two-tailed McNemar test.⁴⁶ To compare the distributions of vertical CDR, we used the Kolmogorov-Smirnov test.⁴⁸ We

measured inter-grader agreement using a weighted Krippendorff's alpha, which is robust to multiple graders.⁴⁹ The weighting function was the diagonal distance (e.g. the distance between the first [non-glaucomatous] and third [high-risk glaucoma suspect] grade is $3-1=2$).

Results

A DL algorithm was developed using a training set of 58,033 fundus images and tuning set of 1,508 fundus images that were assessed for presence of glaucomatous ONH features and overall referable glaucoma risk. The images were graded by a panel of 41 graders using a set of detailed grading guidelines (**Table S1**). Patient demographics and image characteristics for the development and validation sets are summarized in **Table 1**.

Figure 1 summarizes the performance of the algorithm in detecting referable glaucoma risk on a subset of 411 images from validation dataset "A". The algorithm achieved an AUC of 0.938 (95% CI, 0.907-0.964) with sensitivity of 74.6% and specificity of 91.0% at the balanced operating point. The performance of 10 graders on this same subset is plotted for comparison on the ROC curve for algorithm performance (**Figure 1, Table S4**). Performance on the full validation dataset "A" was comparable with an AUC of 0.940 (95% CI, 0.922-0.955), sensitivity of 82.8%, and specificity of 89.2% at the balanced operating point (**Figure S1**).

Graders' sensitivities ranged from 29.2-73.6% (37.5-63.9% for glaucoma specialists, 29.2-73.6% for ophthalmologists and 29.2-70.8% for optometrists) and specificities ranged from 75.8-92.6% (85.5-90.6% for glaucoma specialists, 75.8-90.6% for ophthalmologists and 87.6-92.6% for optometrists). The algorithm was significantly more sensitive than 6 out of 10 graders (2 out of 3 glaucoma specialists). The algorithm had no statistically significant difference in specificity for 9 out of 10 graders, and significantly higher specificity than one ophthalmologist (**Table S4**).

Additionally, we looked at the performance of the algorithm on ONH features (**Table 2**). We also evaluated the relative importance of the different ONH features (**Table 3, Figure S3A-B**). A vertical CDR ≥ 0.7 , presence of a neuroretinal notch, presence of a RNFL defect, and presence of a bared circumlinear vessel had the strongest correlation with an overall assessment of referable glaucoma risk. Presence of a neuroretinal notch, an inferior rim thinner than the superior rim, and presence of a disc hemorrhage (in descending order) had a stronger correlation with the overall referable glaucoma risk of the reference standard labels compared to the round 1 majority grades. See **Table S6** for similar analyses on the training and tuning datasets.

To better understand the association of ONH features with referral, we plotted the distributions of ONH features in the refer and no-refer categories (**Figures 2A, S2**). Most strikingly, the vertical CDR distributions were significantly different between the refer and no-refer categories ($p < 0.001$ for differences in the distribution). We further plotted referral rate as a function of each ONH feature's grade (**Figures 2 and S2**), mimicking a “positive predictive value” analysis of each feature. Marked increases in referral rates were observed when RNFL defect, disc hemorrhage, laminar dot sign and beta PPA were present or possibly present. **Figure 3** summarizes the performance of the algorithm in detecting referable glaucoma risk in validation dataset “B”. For referable glaucoma risk, the algorithm achieved an AUC of 0.858 (95% CI, 0.836-0.878). **Figure 4** includes fundus examples where the algorithm's referral predictions differed from the reference standard in validation dataset “B.”

We further sliced the results for validation dataset “A” based on self-reported sex: the algorithm achieved an AUC of 0.929 (95% CI, 0.900-0.953) for females ($n=569$, **Figure S4A**), and an AUC of 0.943 (95% CI, 0.922-0.955) for males ($n=503$, **Figure S4B**). Validation set “B” had too few females (4.7%) to make the analysis by self-reported sex meaningful.

Discussion

In the present study, we developed and validated a DL algorithm for the prediction of referable glaucoma risk and the prediction of glaucomatous ONH features from fundus images. In addition, we analyzed the relative importance glaucoma specialists attribute to the different features in their overall assessment of referable glaucoma risk.

Performance of the algorithm

Our model achieved an AUC of 0.940 for the detection of referable glaucoma risk. Several previous studies reported similar performance of DL algorithms with AUCs ranging between 0.91-0.986.^{26,28-31} However, these studies suffer from one or more of the following limitations: reference standard images were graded by non-glaucoma specialists limiting the validity of GON identification;^{26,29,31} lack of a consistent definition of glaucoma for the reference standard limiting the effectiveness of algorithm performance evaluation;²⁸ exclusion of low quality images from the training set limiting utility of the algorithm in real life settings;³⁰ exclusion of images where graders had disagreed from the reference standard potentially skewing algorithm performance;³⁰ and the use of fundus images zoomed in on the optic nerve limiting assessment of the RNFL.³¹ Our work advances the field by demonstrating performance on par with or surpassing graders after accounting for all of these limitations.

When evaluated against the referral decisions of eye-care providers in validation dataset “B” (Atlanta VA Eye Clinic diabetic teleretinal program), our algorithm achieved an AUC of 0.858. This decrease in performance relative to validation dataset “A” is likely explained by the difference in reference standard and patient population between the two validation datasets. Graders of validation dataset “A” had access to a single fundus image only from each patient - the same information the algorithm had access to. VA graders of validation dataset “B”, however, had access to the patient’s electronic medical record and therefore to patient history

and previous eye notes containing clinical data - more information than the model had access to. Nonetheless, our algorithm achieved respectable performance in this external validation set for which the reference standard incorporated additional clinical data.

ONH Features analysis

To the best of our knowledge, this is the first study to train an algorithm for the detection of most known glaucomatous ONH features. Our algorithm had good performance in predicting the presence of the different ONH features, with AUCs ranging between 0.608-0.977.

This work allows for a quantitative assessment of the relative importance different ONH features play in the detection of GON by glaucoma specialists and the algorithm. We found that vertical CDR \geq 0.7, presence of a neuroretinal notch, presence of a RNFL defect, and presence of a bared circumlinear vessel were the 4 ONH features most correlated with an overall assessment of referable glaucoma risk, with similar ranking order and coefficients for algorithm predictions and reference standard (as shown in Table 3).

Studies training DL algorithms for glaucoma detection from color fundus images used slightly varying sets of ONH features to determine glaucoma risk, with different thresholds for CDR. Li et al.²⁹ defined “referable GON” as any of the following: CDR $>$ 0.7, rim thinning or notching, disc hemorrhage or RNFL defect. Shibata et al.³⁰ labelled images as “glaucoma” according to the following: focal rim notching or generalized rim thinning, large CDR with cup excavation with/without laminar dot sign, RNFL defects with edges at the optic nerve head margin, disc hemorrhages, and peripapillary atrophy. Ting et al.²⁶ defined “possible glaucoma” if any of the following was present: CDR \geq 0.8, focal thinning or notching of the neuroretinal rim, disc hemorrhages, RNFL defect. Other studies^{28,31} did not report image grading guidelines.

Our findings of CDR, notch and RNFL defect being the top 3 ONH features most correlated with overall glaucoma risk are in line with the approaches described above.

Interestingly, features mostly not assessed in previous studies, i.e. barring of circumlinear vessels, laminar dots (somewhat assessed in Shibata et al.) and nasalization of central ONH vessels, were significantly correlated with overall referable glaucoma risk, while disc hemorrhage was not.

The relatively low ranking of disc hemorrhage in our study can be explained by the study population. Images used in this study were largely derived from diabetic retinopathy screening programs. We asked our graders to mark the presence of any disc hemorrhage, irrespective of its presumed etiology. Therefore, some of the disc hemorrhages identified by our graders may have been due to DR. Our study is the only study to specifically ask graders to assess for the presence of barring of circumlinear vessels (an ONH feature first described by Herschler and Osher in 1980⁵⁰) and nasalization of central ONH vessels (a feature included in the AAO's PPP), both associated with glaucomatous optic nerves, yet are rarely separately delineated by glaucoma specialists in clinical practice. Interestingly, presence of bared circumlinear vessel was among the ONH features highly correlated with overall referable glaucoma risk, while nasalization of central ONH vessels was not. The presence of bared circumlinear vessels is associated with adjacent rim thinning making it a more likely to be correlated with GON than nasalization of central ONH vessels, often seen in large discs.⁵¹

Our findings may be helpful in deciphering the decision making process by which glaucoma specialists identify an ONH as glaucomatous - often previously described by many as a "gut feeling". Understanding which features are most used by glaucoma specialists to grade an optic disc as glaucomatous may help in the development of training programs to enable non-specialists recognize those features in a tele-ophthalmology or screening setting. Similarly, by training the algorithm to detect individual ONH features, we may be able to better explain

what the algorithm's predictions rely on, and thus gain insight into what is frequently referred to as a "black box" of machine learning.

Limitations and future work

Our study has several limitations. First, while ONH assessment for detection of referable glaucoma risk is commonly accepted in screening and teleophthalmology settings, it is well established that subjective evaluation of optic disc photographs suffers from low reproducibility, even when performed by expert graders^{52,53} (e.g. a panel of glaucoma specialists, as done in this study). Second, the diagnosis of glaucoma is not based on ONH appearance alone, but also relies on the compilation of risk factors and repeated clinical, functional and structural testing over time. Thus, the predictions of our algorithm are not diagnostic for glaucoma, but rather are an assessment of the ONH appearance for referable glaucoma risk. A longitudinal dataset consisting of fundus images, clinical exam data, OCT scans and visual field exams could be used to train an algorithm that may be able to diagnose glaucoma, and perhaps even predict progression risk.

Conclusions

We have developed a DL algorithm with higher sensitivity and comparable specificity to eye care providers in detecting referable glaucoma risk in color fundus images. Additionally, our work provides insight into which ONH features are deemed glaucomatous by glaucoma specialists. We believe that an algorithm trained to accurately predict referable glaucoma risk from color fundus images may enable effective population-wide screening for glaucoma. The utilization of such a tool presents an opportunity to reach underserved populations world-wide.

Acknowledgements

Google AI Healthcare: William Chen BS, Quang Duong PhD, Xiang Ji MS, Jess Yoshimi BS, Cristhian Cruz MS, Olga Kanzheleva MS, Miles Hutson BS, Brian Basham BS.

EyePACS: Jorge Cuadros, OD, PhD

This research has been conducted using the UK Biobank Resource under Application Number 17643.

Tables and figures

Table 1. Baseline Characteristics				
Characteristics	Development Datasets*		Validation Dataset A	Validation Dataset B VA Atlanta
	Training dataset	Tuning Dataset		
No. of images (1 image per patient, except Validation Dataset B)	58,033	1,508	1,205	17,593
No. of graders	41 graders: 13 glaucoma specialists; 25 ophthalmologists; 3 optometrists	11 glaucoma specialists	12 glaucoma specialists	6 ophthalmologists
No. of grades per image	1-2	3	3-6	1
Grades per grader, median (IQR)	659 (188-2256)	388 (96-553)	185 (93-731)	1
Patient demographics				
No. of patients	58,033	1,508	1,205	9,643
Age, median (IQR); no. of images for which age was available	58 (49-65); 43,051	57 (49-64.8); 1,386	57 (49.5-64); 1,115	64 (68.7-57.5); 9,643
Females, No./total of images for which sex was known (%)	21,230/41,211 (51.5)	731/1,349 (54.2)	570/1,071 (53.2)	457/9,643 (4.7)
Glaucoma Gradability distribution				
Images gradable for glaucoma, No./total (%) among images for which glaucoma gradability was assessed	48,800/57,542 (84.8)	1,451/1,508 (96.2)	1,171/1,204 (97.3)	17,593/17,593 (100)**
Glaucoma risk assessment distribution				
No. non-Glaucomatous (%)	20,303 (41.5)	849 (57.1)	687 (57.5)	8,753 (90.8)

No. low-risk glaucoma suspect (%)	14,314 (29.3)	259 (17.4)	290 (24.3)	N/A***
No .high-risk glaucoma suspect (%)	10,128 (20.7)	268 (18.0)	170 (14.1)	N/A***
No. likely glaucoma (%)	4,160 (11.0)	110 (7.4)	48 (4.0)	890 (9.2)
No. "Referable glaucoma" (%)	14,288 (31.7)	378 (25.4)	218 (18.1)	890 (9.2)

Abbreviations: VA, Veterans Affairs; IQR, Interquartile Range;

* prevalence of referable glaucoma risk images is higher than in the general population in part due to active learning, a machine learning technique used to preferentially increase the number of relevant examples (methods).

** all images in validation set B were of overall "adequate image quality", but not specifically labeled by graders for glaucoma gradability.

*** finer-grained categorization not available, see Methods

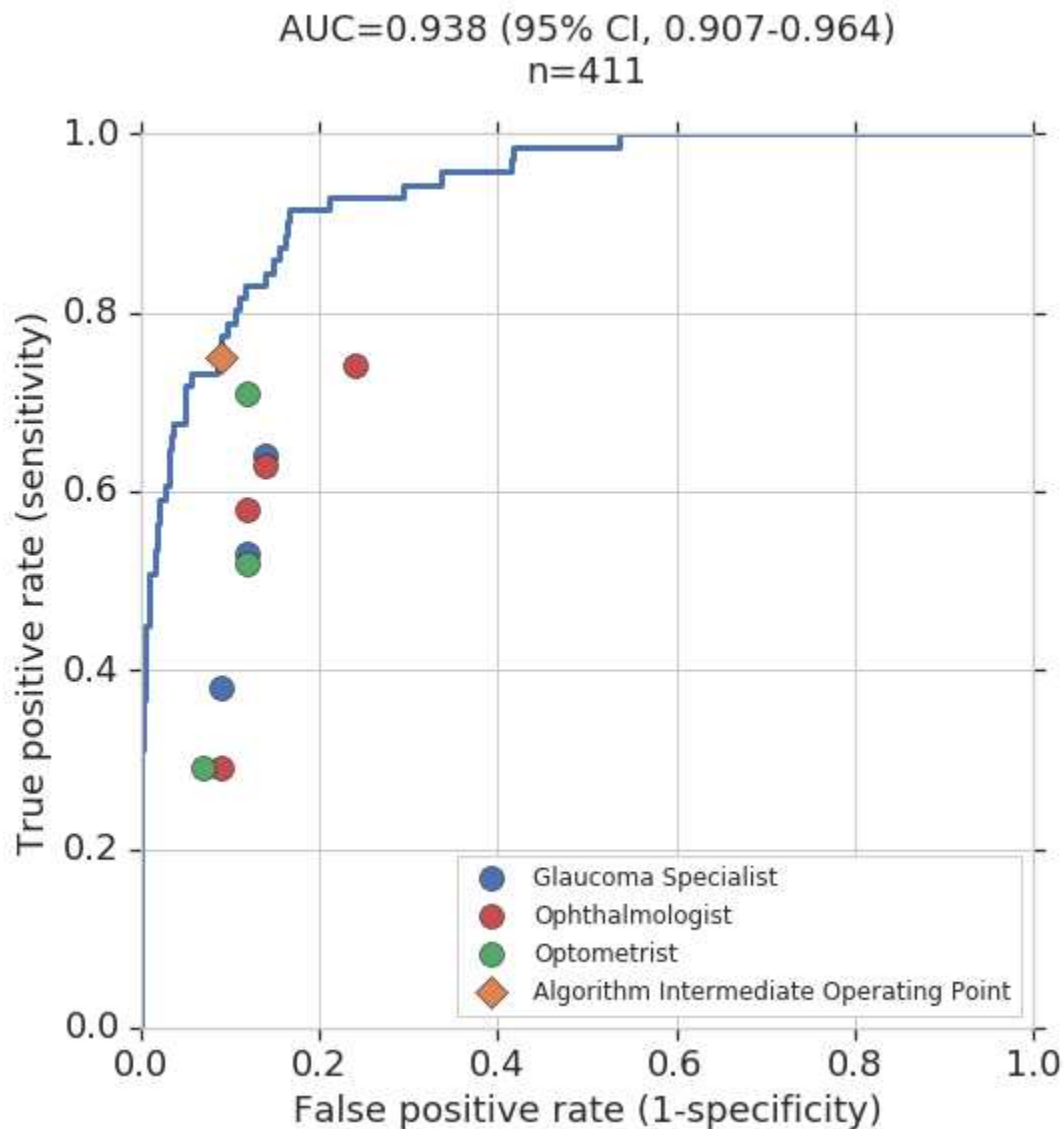


Figure 1. Receiver operating characteristic curve (ROC) analysis for referable Glaucoma in a subset of validation dataset A (n=411) with human evaluation.

The algorithm is illustrated as a blue line, with 10 individual graders indicated by colored dots: glaucoma-specialists (blue), ophthalmologists (red), and optometrists (green). The diamond corresponds to the balanced operating point of the algorithm, chosen based on performance on the tuning set. For each image, the reference standard was determined by a different set of three glaucoma specialists in an adjudication panel (Methods). Images labeled by graders as ‘ungradable’ for glaucoma, were considered as ‘refer’ to enable comparison on the same set of images. For a sensitivity analysis excluding the ‘ungradable’ images on a per-grader basis, see **Table S5**. See **Figure S1** for analysis on the entire validation dataset “A.”

Table 2. Evaluation of Algorithm Performance for Detecting Presence of Individual Features on Validation Dataset A

	AUC [95% CI]	Number of labeled images	Prevalence (%)	Binary cutoffs
Rim width I Vs. S	0.608 [0.567-0.648]	1,162	25.9	I<S or I~S vs. I>S
Rim width S Vs. T	0.801 [0.774-0.827]	1,156	71.5	S<T or S~T vs. S>T
Notch	0.927 [0.867-0.980]	1,162	2.6	Yes/Possible vs. No
Laminar dot sign	0.957 [0.944-0.968]	1,013	24	Yes/Possible vs. No
Nasalization emerging	0.977 [0.962-0.990]	1,166	4.7	Yes vs. Possible/No
Nasalization directed	0.971 [0.961-0.981]	1,167	15.9	Yes vs. Possible/No
Baring of circumlinear vessels	0.744 [0.694-0.973]	1,154	10.8	Present and clearly bared vs. All else
Disc hemorrhage	0.788 [0.684-0.981]	1,173	2.1	Yes/Possible vs. No
Beta PPA	0.945 [0.932-0.960]	1,170	16.9	Yes/Possible vs. No
RNFL defect	0.797 [0.719-0.866]	973	6.5	Yes/Possible vs. No
Vertical CD ratio	0.793 [0.681-0.801]	1,154	5.9	≥0.7 vs. <0.7

Abbreviations: AUC, Area Under the Curve; CI, Confidence interval; I, Inferior; S, Superior; T, Temporal; PPA, ParaPapillary Atrophy; RNFL, Retinal Nerve Fiber Layer; CD, Cup-to-Disc

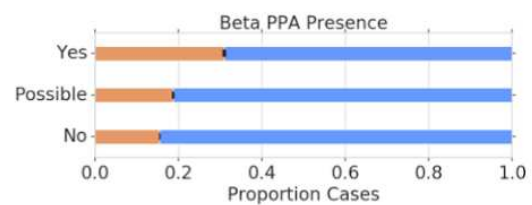
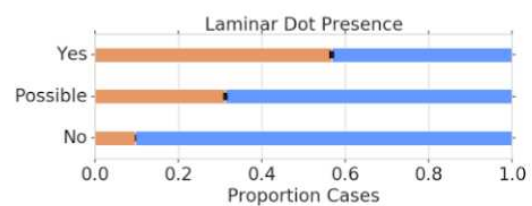
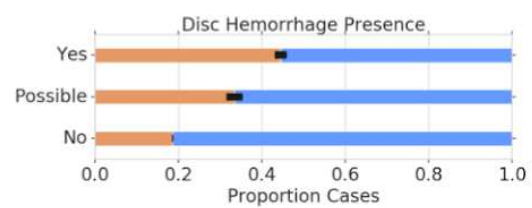
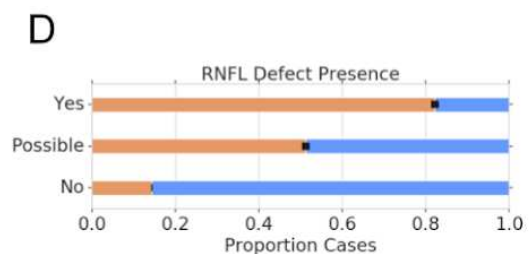
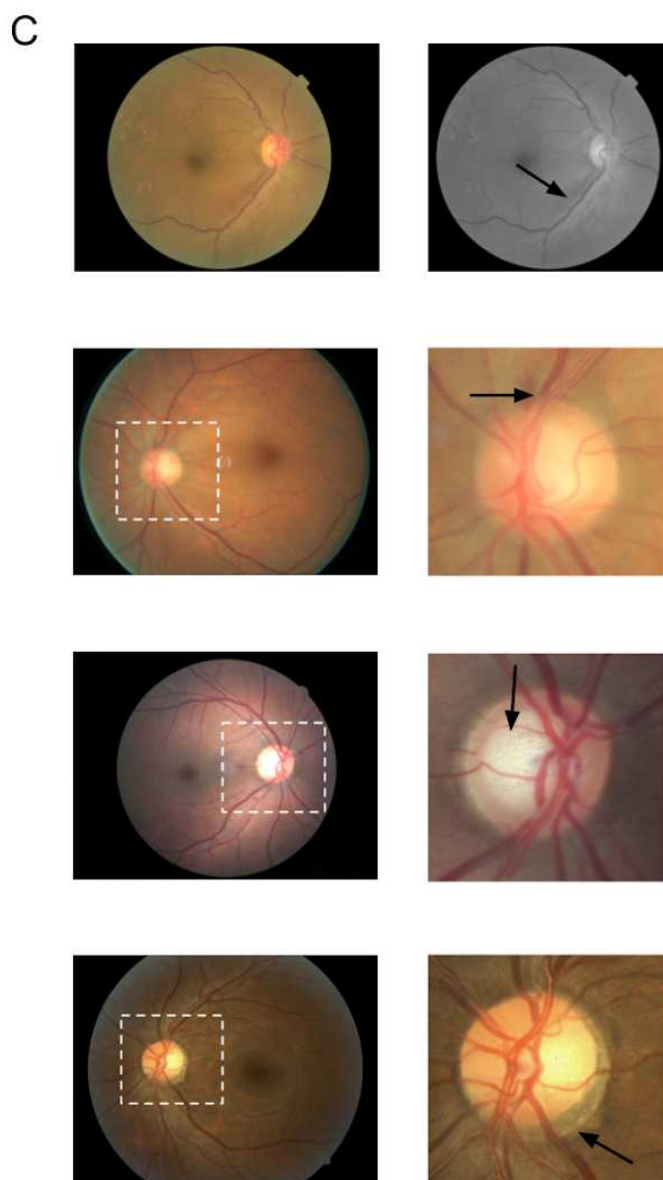
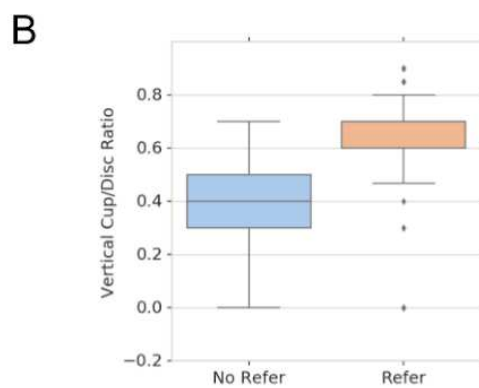
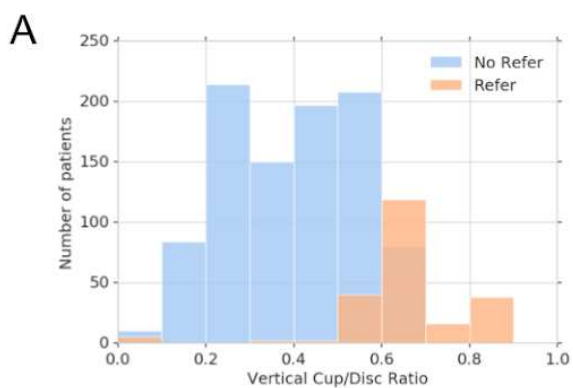
Table 3. Logistic Regression Models to Understand the Relative Importance of Individual Optic Nerve Head Features for Glaucoma Referral Decisions in Validation Dataset A: The Reference Standard, Algorithm Predictions, and Round 1 Majority (N=1015)*

	Reference Standard			Algorithm Predictions			Round 1 Majority		
	Odds Ratio	p-value	Rank	Odds Ratio	p-value	Rank	Odds Ratio	p-value	Rank
Vertical CD Ratio ≥ 0.7	428.028 [†]	<0.001	1	330.005 [†]	<0.001	1	461.891 [†]	<0.001	1
Notch: Possible or Yes	21.175	<0.001	2	7.910	0.041	3	3.830	0.267	4
RNFL Defect: Possible or Yes	10.427	<0.001	3	12.788	<0.001	2	14.110	<0.001	2
Circumlinear Vessels: Present + Bared	5.723	<0.001	4	7.783	<0.001	4	6.303	<0.001	3
Rim I/S Comparison: I < S	3.662	<0.001	5	4.507	<0.001	5	2.959	0.002	7
Laminar Dot: Possible or Yes	3.272	<0.001	6	2.982	<0.001	8	3.390	<0.001	6
Disc Hemorrhage: Possible or Yes	2.779	0.085	7	1.949	0.440	9	1.557	0.563	10
Nasalization Directed: Yes	2.545	<0.001	8	3.111	<0.001	7	2.329	<0.001	8
Nasalization Emerging: Yes	2.146	0.091	9	3.553	0.006	6	3.542	0.001	5
Beta PPA: Yes	1.935	0.013	10	1.695	0.076	10	1.683	0.037	9
Circumlinear Vessels: Present, Not Bared	1.200	0.544	11	1.419	0.254	11	1.516	0.114	11
Rim S/T Comparison: S < T	1.070	0.963	12	1.007	0.997	12	0.965	0.982	12

Abbreviations: CD, Cup-to-Disc; RNFL, Retinal Nerve Fiber Layer; I, Inferior; S, Superior; PPA, ParaPapillary Atrophy; T, Temporal;

[†]: Extreme odds ratios here indicate almost perfect correlation between the feature and the final referral prediction or grade.

* Some images in Validation Set A were excluded from analysis due to being ungradable on referral criteria or for a specific ONH feature.



Refer (Orange)
No Refer (Blue)

Figure 2A-D: Proportions of selected Optic Nerve Head feature grades amongst the refer/no-refer categories in validation data set “A”.

(A) Counts of patients with a vertical cup-to-disc-ratio by refer/no-refer categories of glaucoma risk.

(B) Box-plot of Vertical cup-to-disc-ratio by refer/no-refer categories of glaucoma risk.

(C) ONH feature example images for RNFL defect, Disc hemorrhage, Laminar dot sign and Beta PPA.

(D) Corresponding distributions of ONH feature presence by refer/no-refer categories of glaucoma risk. Error bars represent 95% binomial confidence intervals on the proportion of cases with referable glaucoma.

Abbreviations: ONH, Optic Nerve Head; RNFL, Retinal Nerve Fiber Layer; PPA, ParaPapillary Atrophy

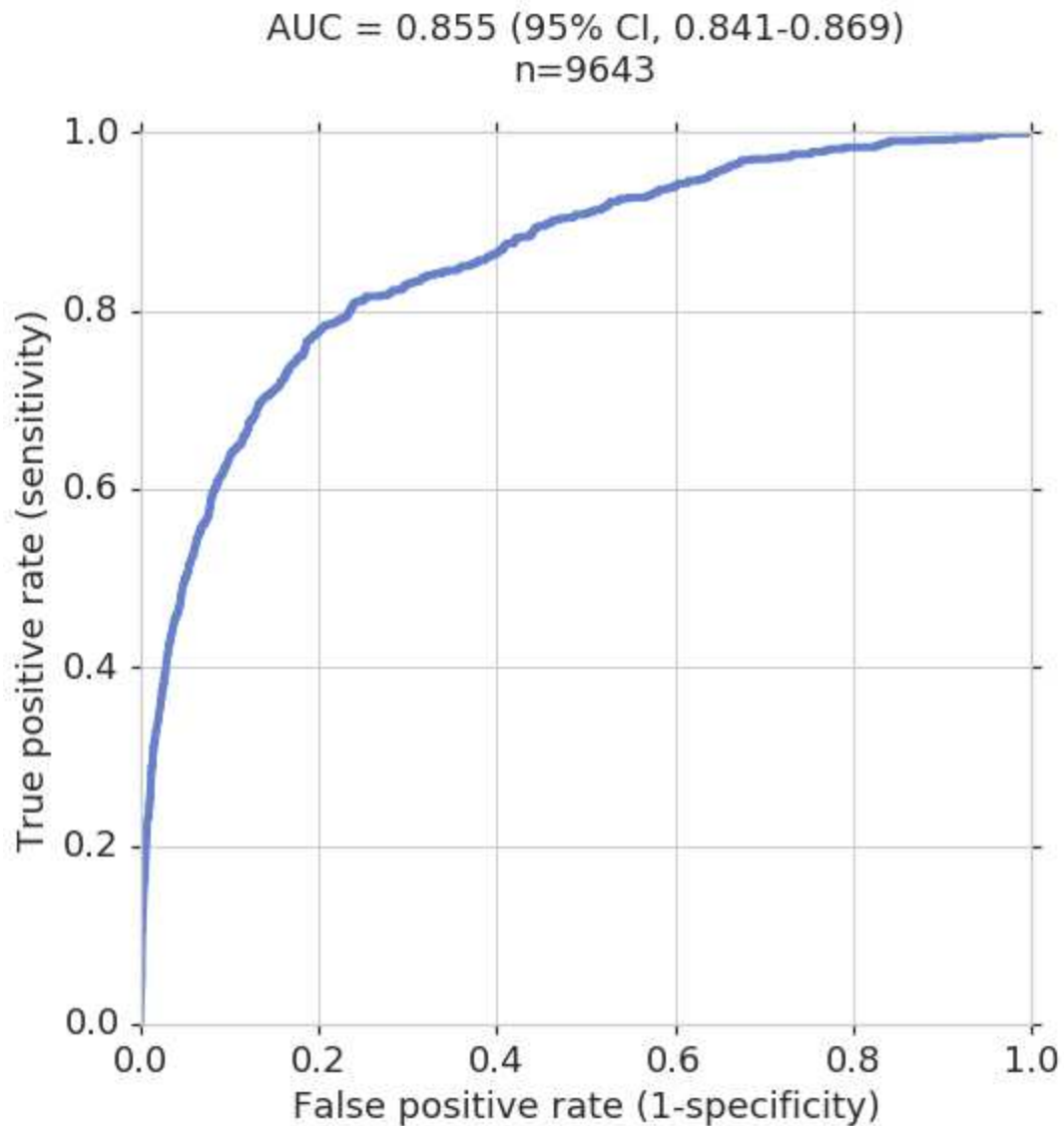

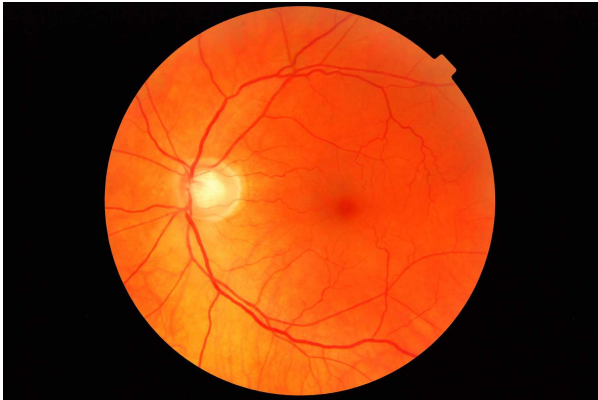

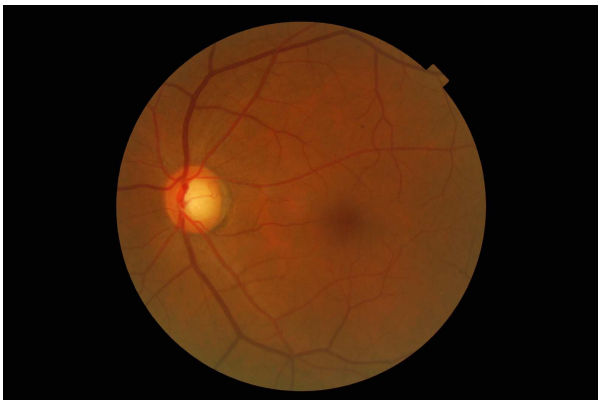




Figure 3. Receiver operating characteristic curve (ROC) analysis for referable Glaucoma in validation dataset “B” (VA Atlanta).

The ROC curve of the algorithm in predicting referable Glaucoma is plotted as the blue line. In validation dataset B, the reference standard for all images was determined by glaucoma related ICD codes.

<p>False Positive</p>  <p>Actual: No refer Predicted: Refer</p>	<p>False Positive</p>  <p>Actual: No refer Predicted: Refer</p>
<p>False Positive</p>  <p>Actual: No refer Predicted: Refer</p>	<p>False Positive</p>  <p>Actual: No refer Predicted: Refer</p>
<p>False Negative</p>  <p>Actual: Image taken 618 days prior to ICD glaucoma code Predicted: No Refer</p>	<p>False Negative</p>  <p>Actual: Image taken 1 day prior to ICD glaucoma code Predicted: No Refer</p>
<p>False Negative</p>	<p>False Negative</p>

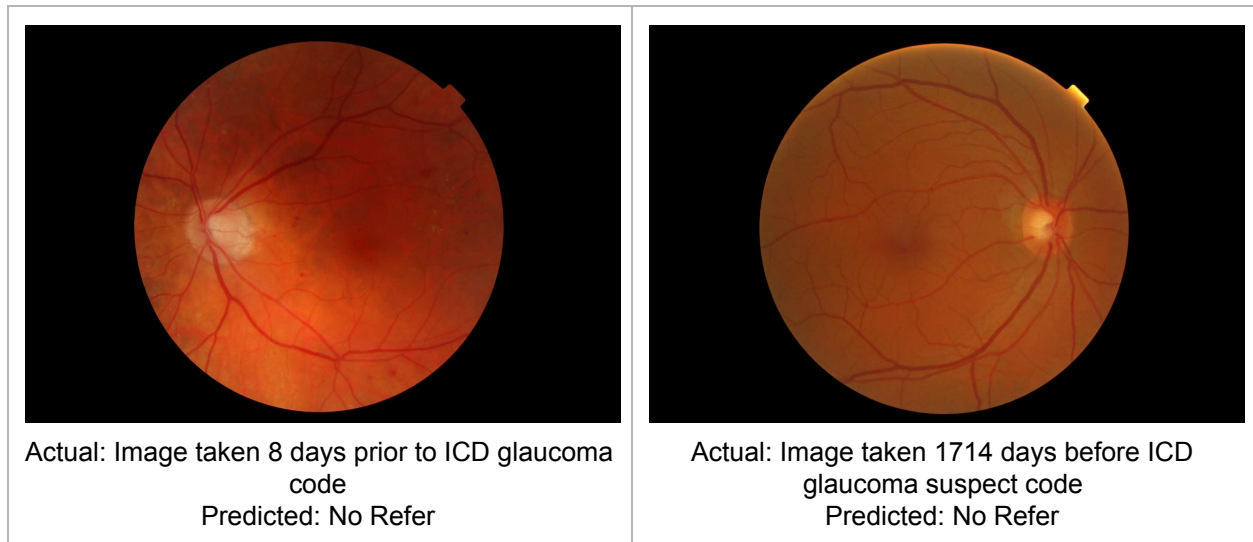


Figure 4. Examples of incorrect algorithm predictions.

Images had a referral prediction different than the reference standard for validation set “B”.

Discrepancies between ONH appearance and VA diabetic teleretinal screening program glaucoma referral decisions may be explained by VA providers’ access to clinical data available in patients’ electronic medical records.

Abbreviations: ICD, International Classification of Diseases; ONH, Optic nerve head

Supplement

Table S1. Grading Guidelines		
	Question	Possible answers
Optic nerve head features		
Rim width assessment	Is the inferior rim (I) width greater than the superior rim (S) width?	<u>I clearly greater than S</u> : Inferior rim width is greater than superior rim width (the ratio I:S is 3:2 or more*) <u>Similar widths</u> : Inferior and superior rim widths are roughly the same <u>S clearly greater than I</u> : Superior rim width is greater than inferior rim width (the ratio S:I is 3:2 or more*)
	Is the superior rim (S) width greater than the temporal rim (T) width?	<u>S clearly greater than T</u> : Superior rim width is greater than temporal rim width (the ratio S:T is 3:2 or more*) <u>Similar widths</u> : Superior and temporal rim widths are roughly the same <u>T clearly greater than S</u> : Temporal rim width is greater than superior rim width (the ratio T:S is 3:2 or more*)
	Is there a notch in the neuroretinal rim?	<u>Yes</u> : A notch in the neuroretinal rim is present that: - has circumferential extent of up to 3 clock hours - has a change in curvature - does not fall only in the temporal quadrant <u>Possible</u> : Possible notch that is borderline on criteria for Yes <u>No</u> : No notch in the neuroretinal rim is present - Notch is entirely in the temporal quadrant (9 o'clock OD, 3 o'clock OS) should be marked as [No]
Laminar dot sign	Are laminar dots or striations visible?	<u>Yes</u> : Laminar dots/striations are visible within the cup <u>Subtle/Possible</u> : Possible laminar dots/striations visible within the cup <u>No</u> : No dots or striations present
Nasalization of central vascular trunk	Is central trunk emerging in the nasal third of the optic nerve head?	<u>Yes</u> : Central vascular trunk is emerging in nasal third of disc <u>Borderline</u> : Central trunk is emerging at the border of the central and nasal thirds, or Vein emerges in central third and artery emerges in nasal third <u>No</u> : Central trunk is emerging in the central or temporal thirds
	Is central vascular trunk directed nasally?	<u>Yes</u> : Central vascular trunk is directed nasally <u>minimally</u> : Central vascular trunk is minimally directed nasally <u>No</u> : Central vascular trunk is not directed nasally
Baring of	Are bared circumlinear	<u>Present & Clearly not bared</u> : Obvious circumlinear

circumlinear vessels	vessels present?	vessel/s are present and clearly none are bared <u>Present & Clearly bared</u> : Obvious circumlinear vessel/s are present and clearly at least one is bared <u>Possibly present or possibly bared</u> : circumlinear vessel possibly present or an obvious circumlinear vessel is possibly bared <u>No circumlinear vessels present</u> : No circumlinear vessels are present
Disc hemorrhage	Is a hemorrhage at /near the disc present?	<u>Yes</u> : A hemorrhage at or near the disc is present that is within 2 vessel widths from the edge of the disc <u>Possible/Borderline</u> : Heme that is borderline on criteria for Yes or possible heme that meets criteria <u>No</u> : No hemorrhage at/near the neuroretinal rim
Beta PPA	Is beta PPA present?	<u>Yes</u> : Beta PPA is present (with or without alpha) <u>Possible</u> : PPA is possibly present (e.g. atypical location, not sure if its alpha or Beta, etc.) <u>No</u> : there is only alpha PPA, or there is no PPA at all
RNFL defect	Is an RNFL defect present?	<u>Yes</u> : RNFL defect is present that: - follows an arcuate pattern - extends all the way to the disc - is wedge shaped, narrows as it gets closer to disc or RNFL loss is such that only one clear sheen/RNFL absence border is seen <u>Possible</u> : Possible RNFL defect that is borderline on criteria for Yes <u>No</u> : No RNFL defect present
Vertical cup-to-disc ratio	Estimate the vertical cup-to-disc ratio to nearest 0.1	0.1-0.9
Glaucoma risk		
Risk assessment	Estimate risk for glaucoma	<u>Non-glaucomatous</u> : disc does not appear glaucomatous; No need for OCT / VF to rule out glaucoma; Follow up in about 2 years <u>Low-risk glaucoma suspect</u> : Unlikely to have glaucoma but not completely normal; Order baseline VF and OCT if had the resources available; Follow up about 1 year <u>High-risk glaucoma suspect</u> : Even chance to likely to have glaucoma; Order serial VFs and OCTs if had the resources available; Follow up about 4-6 months <u>Likely glaucoma</u> : Almost certain to have glaucoma; Order serial VFs and OCTs if had the resources available; Probably needs treatment now
Other ONH findings		
Assessment of	Pallor out of proportion to	Yes

ONH for presence of additional findings	cupping	No
	Disc swelling	Yes No
	Optic nerve head tumor	Yes No
	Melanocytoma	Yes No
	Disc drusen	Yes No
	Anomalous disc	Yes No
	Other findings?	Free-text box

Abbreviations: PPA, ParaPapillary Atrophy; RNFL, Retinal Nerve Fiber Layer; ONH, Optic Nerve Head; OCT, Optical Coherence Tomography; VF, Visual Field.

Data pre-processing

For algorithm training, input images were scale normalized by detecting the circular mask of the fundus image and resizing the diameter of the fundus to be 587 pixels wide. Images for which the circular mask could not be detected were not used in the development, tuning, or clinical validation sets.

Images from validation set B were all chosen from the macula centered fundus field. If an “optic nerve head” referral code was present, then images from that visit were chosen. In cases where a glaucoma-related ICD code was present and there were multiple images, the image selected was the one with the date closest to the glaucoma ICD code date, up to one year after the ICD code was given.

Tuning Dataset

In algorithm development, the performance on the tuning set was used to select the algorithm checkpoint that yielded the highest AUC for referable glaucoma risk. Once a checkpoint was determined, operating points at high sensitivity, high specificity, and a balanced point were chosen, and the thresholds at these values were then applied during evaluation on the validation sets. The balanced point was chosen to be a point with reasonable sensitivity and specificity on the tuning set.

The tuning set was independently graded by three glaucoma specialists. Since this set was not adjudicated, a majority vote was used.

Table S2. Comparison of Round 1, Round 2 (Reference Standard), and Fully Adjudicated Grades in a Set of 100 Images									
		Round 1				Round 2 (Reference Standard)			
		Non-glaucoma	Low-risk	High-risk	Likely	Non-glaucoma	Low-risk	High-risk	Likely
Fully adjudicated values	Non-glaucoma	37	0	0	0	36	0	0	0
	Low-risk	6	26	0	0	2	29	0	0
	High-risk	1	1	14	0	0	1	13	0
	Likely glaucoma	0	1	0	4	0	0	0	5

A set of 100 images was fully adjudicated. Compared to the round 1 “median” (see Methods), 9 images had altered grades (in bold), changing referral decisions for 3 (bolded and underlined). Compared to the round 2 median, 3 images had altered grades (in bold), changing referral decisions for only 1 of the 100 images (bolded and underlined). Thus the round 2 median was used as the reference standard.

Table S3. Intergrader agreement on round 1 and round 2 as measured against the Reference Standard in a set of 100 images		
	Krippendorff's alpha values*	
Question	Round 1	Round 2
Referable glaucoma risk	0.89	0.98
Glaucoma gradability	0.87	0.98
Rim width comparison - inferior vs. superior	0.84	0.88
Rim width comparison - superior vs. temporal	0.76	0.94
Rim notching	0.66	0.76
RNFL defect	0.94	0.94
Disc hemorrhage	0.77	0.90
Laminar dot sign	0.94	1.0
Nasalization of central vascular trunk	0.85	0.95
Baring of circumlinear vessels	0.92	0.93

Abbreviations: RNFL, Retinal Nerve Fiber Layer;

* good agreement for Krippendorff's alpha (Landis and Koch)

0 to .2 "slight"; 0.21 to 0.40 "fair"; 0.41 to 0.60 "moderate"; 0.61 - 0.80 "substantial"; 0.81 to 1 "near perfect"

Table S4. Sensitivity and Specificity of Graders Versus Algorithm Performance on Validation Dataset A				
Grader/Algorithm	Sensitivity [95% CI]	p-value	Specificity [95% CI]	p-value
Algorithm (Balanced Operating Point)	0.746 [0.630 - 0.842]	Reference point	0.910 [0.875 - 0.938]	Reference point
Algorithm (High Sensitivity Operating Point)	0.845 [0.741 - 0.920]	N/A	0.858 [0.816 - 0.893]	N/A
Algorithm (High Specificity Operating Point)	0.634 [0.512 - 0.744]	N/A	0.969 [0.945 - 0.985]	N/A
Glaucoma Specialist 1	0.639 [0.517 - 0.749]	0.152	0.855 [0.813 - 0.891]	0.126
Glaucoma Specialist 2	0.528 [0.407 - 0.647]	0.003	0.882 [0.843 - 0.914]	0.766
Glaucoma Specialist 3	0.375 [0.264 - 0.497]	< 0.001	0.906 [0.869 - 0.935]	0.542
Ophthalmologist 1	0.625 [0.503 - 0.736]	0.064	0.855 [0.813 - 0.891]	0.081
Ophthalmologist 2	0.292 [0.190 - 0.411]	< 0.001	0.906 [0.869 - 0.935]	0.542
Ophthalmologist 3	0.583 [0.461 - 0.698]	0.008	0.885 [0.846 - 0.917]	0.883
Ophthalmologist 4	0.736 [0.619 - 0.833]	1	0.758 [0.709 - 0.803]	<0.001
Optometrist 1	0.514 [0.393 - 0.633]	0.002	0.882 [0.843 - 0.914]	0.761
Optometrist 2	0.708 [0.589 - 0.810]	0.629	0.876 [0.836 - 0.909]	0.522
Optometrist 3	0.292 [0.190 - 0.411]	< 0.001	0.926 [0.893 - 0.952]	0.073

Abbreviations: CI, Confidence interval;

Table S5. Sensitivity And Specificity of Graders Versus Algorithm Performance on Subset they Deemed Gradable							
Grader	Number deemed gradable	Sensitivity [95% CI]	Sensitivity of Algorithm* [95% CI]	p-value*	Specificity [95% CI]	Specificity of Algorithm* [95% CI]	p-value*
Glaucoma Specialist 1	391	0.639 [0.517 - 0.749]	0.746 [0.629 - 0.842]	0.152	0.912 [0.875 - 0.941]	0.915 [0.879 - 0.943]	1
Glaucoma Specialist 2	386	0.528 [0.407 - 0.647]	0.746 [0.629 - 0.842]	0.003	0.955 [0.926 - 0.975]	0.907 [0.870 - 0.937]	0.006
Glaucoma Specialist 3	397	0.375 [0.264 - 0.497]	0.746 [0.629 - 0.842]	<0.001	0.948 [0.917 - 0.969]	0.907 [0.870 - 0.937]	0.041
Ophthalmologist 1	398	0.625 [0.503 - 0.736]	0.746 [0.629 - 0.842]	0.064	0.892 [0.853 - 0.924]	0.911 [0.874 - 0.939]	0.392
Ophthalmologist 2	392	0.292 [0.190 - 0.411]	0.746 [0.629 - 0.842]	<0.001	0.962 [0.935 - 0.980]	0.906 [0.868 - 0.936]	0.001
Ophthalmologist 3	382	0.571 [0.447 - 0.689]	0.754 [0.635 - 0.849]	0.002	0.965 [0.938 - 0.982]	0.913 [0.876 - 0.942]	0.004
Ophthalmologist 4	389	0.729 [0.609 - 0.828]	0.768 [0.651 - 0.861]	0.581	0.808 [0.761 - 0.850]	0.912 [0.875 - 0.941]	<0.001
Optometrist 1	395	0.514 [0.393 - 0.633]	0.746 [0.629 - 0.842]	0.002	0.929 [0.895 - 0.954]	0.910 [0.873 - 0.939]	0.392
Optometrist 2	390	0.704 [0.584 - 0.807]	0.757 [0.640 - 0.852]	0.455	0.934 [0.901 - 0.959]	0.906 [0.868 - 0.935]	0.108
Optometrist 3	386	0.250 [0.153 - 0.370]	0.791 [0.674 - 0.881]	<0.001	0.991 [0.973 - 0.998]	0.918 [0.882 - 0.946]	<0.001

Abbreviations: CI, Confidence interval;

* Algorithm was evaluated at the balanced operating point on the subset graders deemed gradable, and p-value is a comparison to this point

Table S6. Logistic Regression Models to Understand the Relative Importance of Individual Optic Nerve Head Features for Glaucoma Referral Decisions in the development sets						
	Train Set (N=44,244)			Tuning Set (N=1,203)		
	Odds Ratio	p-value	Rank	Odds Ratio	p-value	Rank
Vertical CD Ratio ≥ 0.7	30.063	<0.001	1	158.042	<0.001	1
RNFL Defect: Possible or Yes	4.123	<0.001	2	9.336	<0.001	3
Notch: Possible or Yes	3.891	<0.001	3	3.210	0.236	6
Rim S/T Comparison: S < T	2.191	<0.001	4	2.157	0.341	9
Nasalization Directed: Yes	2.063	<0.001	5	2.223	<0.001	8
Laminar Dot: Possible or Yes	1.944	<0.001	6	3.378	<0.001	4
Nasalization Emerging: Yes	1.842	<0.001	7	3.332	0.001	5
Rim I/S Comparison: I < S	1.773	<0.001	8	2.051	0.035	10
Circumlinear Vessels: Present + Bared	1.534	<0.001	9	9.426	<0.001	2
Disc Hemorrhage: Possible or Yes	1.501	<0.001	10	1.538	0.585	11
Rim I/S Comparison: I > S	1.096	0.003	11	1.124	0.632	12
Beta PPA: Yes	1.017	0.602	12	2.870	<0.001	7
Rim S/T Comparison: S > T	0.927	0.011	13	0.500	0.002	14
Circumlinear Vessels: Present, not Bared	0.502	<0.001	14	1.077	0.756	13

Abbreviations: Sig., Significance; CD, Cup-to-disc; RNFL, Retinal Nerve Fiber Layer; S, Superior; T, Temporal; I, Inferior; PPA, ParaPapillary Atrophy;

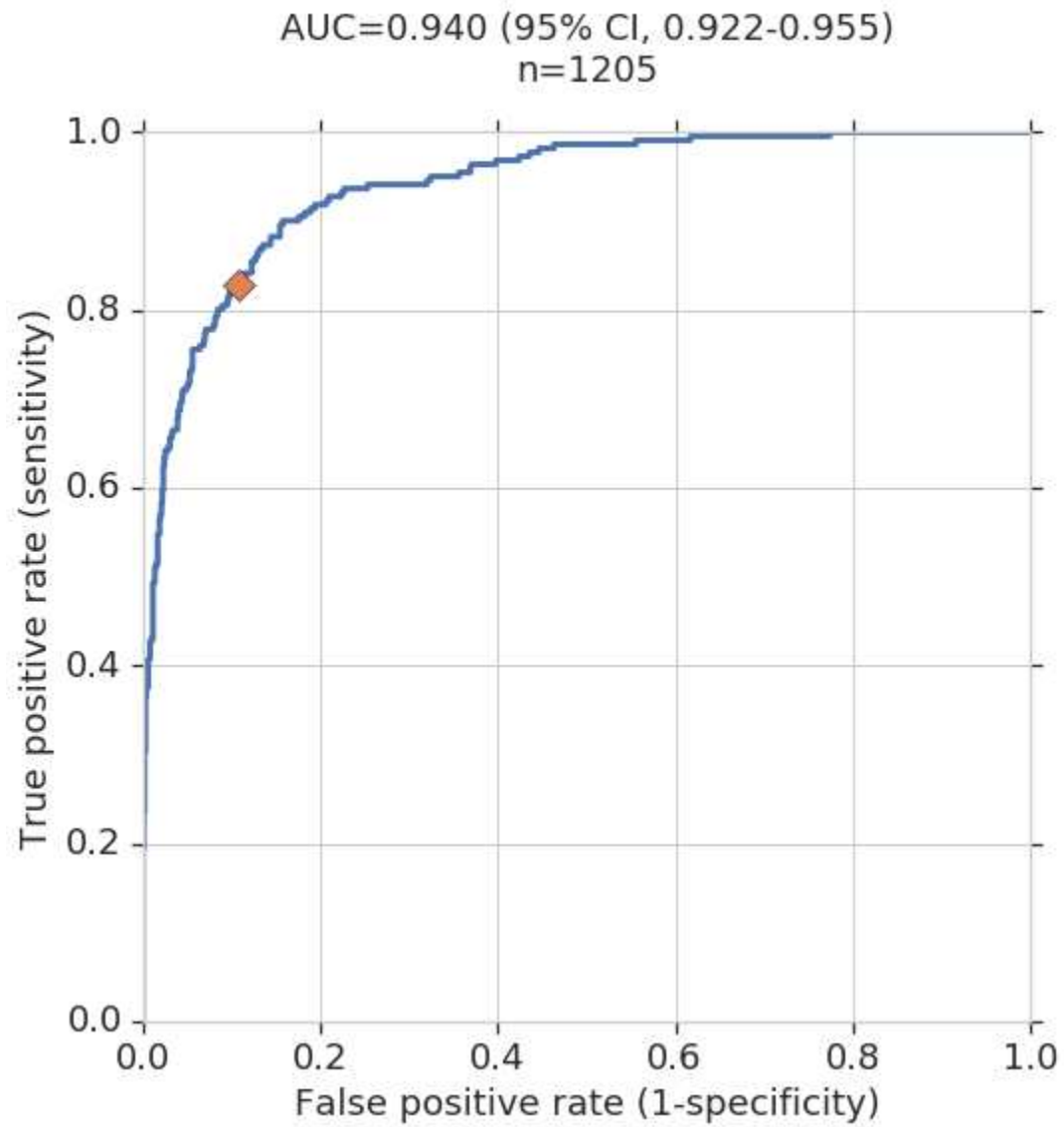


Figure S1. Receiver operating characteristic curve (ROC) analysis for referable Glaucoma in validation dataset A (n=1205).

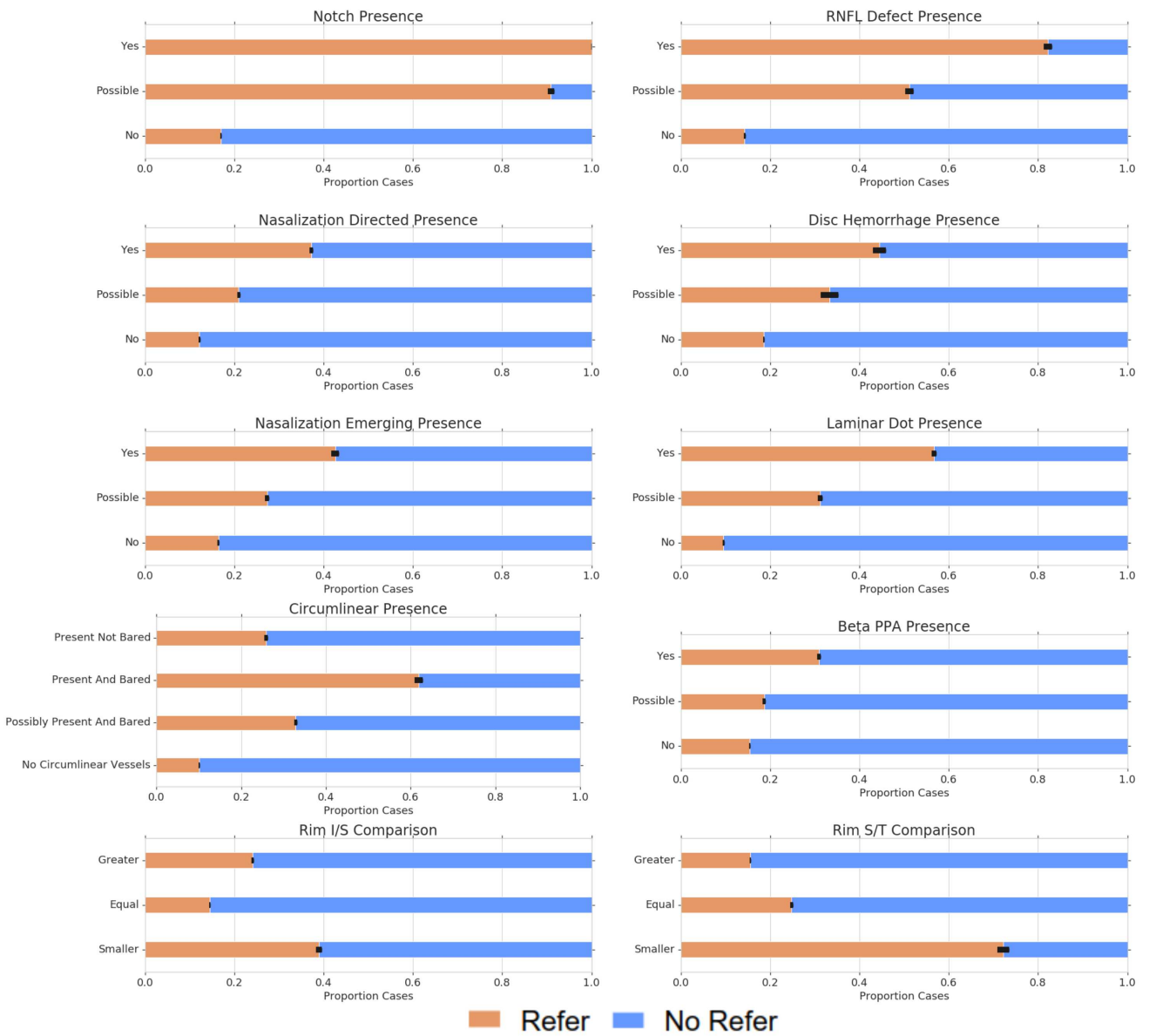


Figure S2: Proportions of all ONH feature grades amongst refer/no-refer from validation dataset "A". Error bars represent 95% binomial confidence intervals on the proportion of cases with referable glaucoma.
Abbreviations: ONH

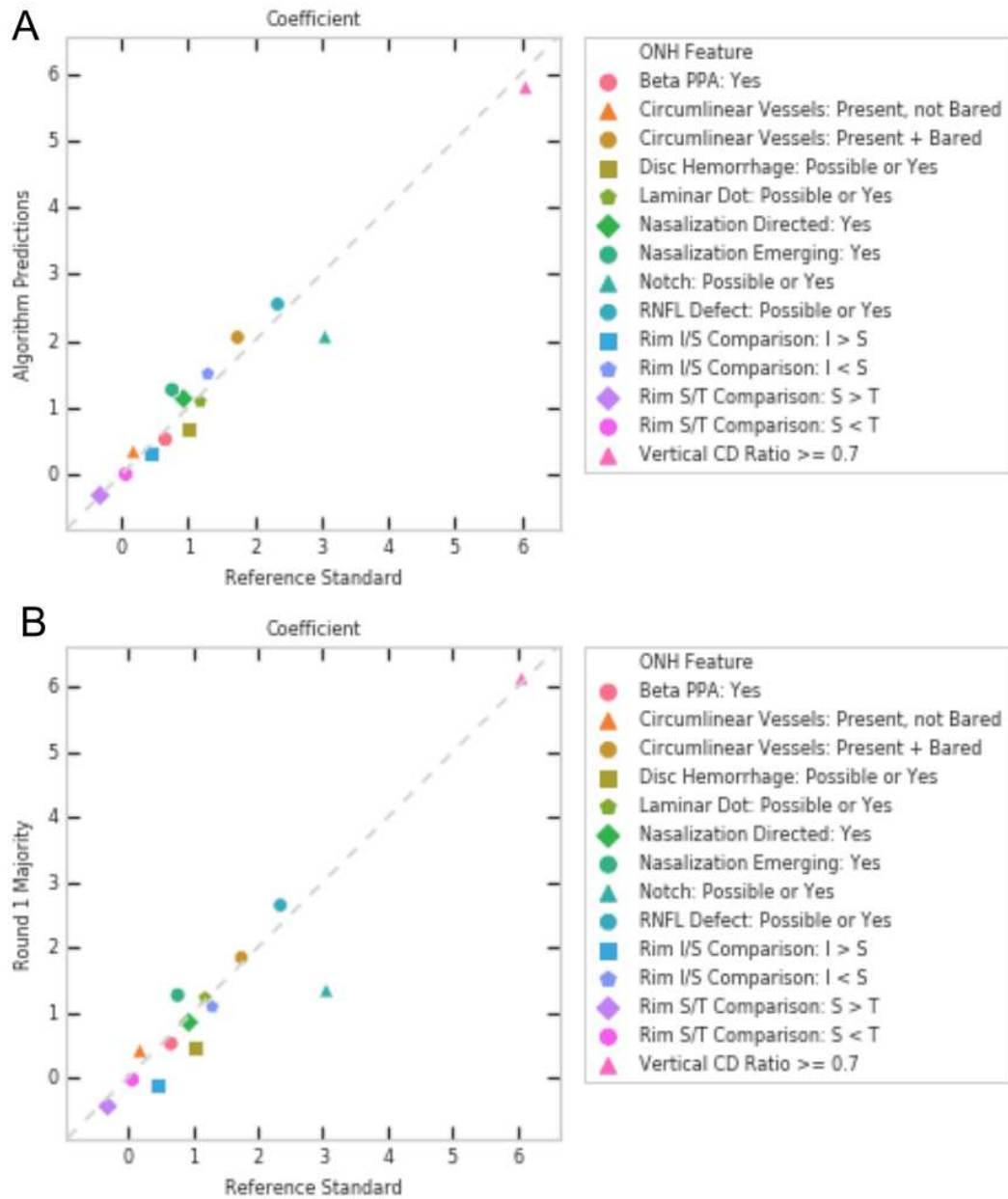


Figure S3A-B: Comparison of the relative importance of ONH features for refer/no-refer decisions in (A) Algorithm Predictions vs. Reference Standard and (B) Round 1 Majority vs. Reference Standard. Feature importance is quantified as the beta coefficient from the corresponding logistic regression (Table 3).

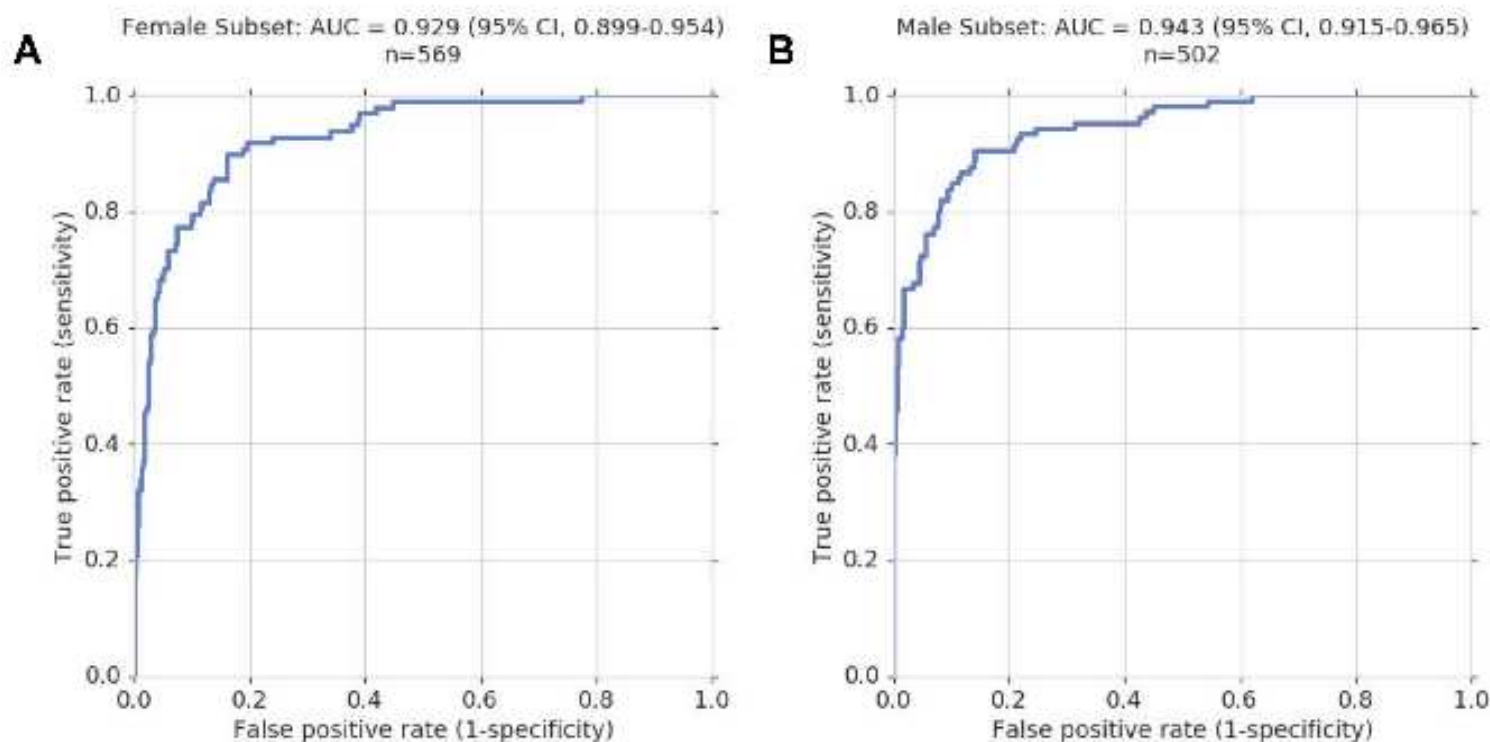


Figure S4A-B: Receiver operating characteristic curve (ROC) analyses for referable Glaucoma in subsets of validation dataset A with only females (n=569) (A) and only males (n=502) (B). Self-reported sex was only available for 1,071 images.

References

1. Quigley HA, Broman AT. The number of people with glaucoma worldwide in 2010 and 2020. *Br J Ophthalmol*. 2006;90(3):262-267.
2. Tham Y-C, Li X, Wong TY, Quigley HA, Aung T, Cheng C-Y. Global prevalence of glaucoma and projections of glaucoma burden through 2040: a systematic review and meta-analysis. *Ophthalmology*. 2014;121(11):2081-2090.
3. Leite MT, Sakata LM, Medeiros FA. Managing glaucoma in developing countries. *Arq Bras Oftalmol*. 2011;74(2):83-84.
4. Rotchford AP, Kirwan JF, Muller MA, Johnson GJ, Roux P. Temba glaucoma study: a population-based cross-sectional survey in urban South Africa. *Ophthalmology*. 2003;110(2):376-382.
5. Hennis A, Wu S-Y, Nemesure B, Honkanen R, Cristina Leske M. Awareness of Incident Open-angle Glaucoma in a Population Study. *Ophthalmology*. 2007;114(10):1816-1821.
6. Prum BE Jr, Lim MC, Mansberger SL, et al. Primary Open-Angle Glaucoma Suspect Preferred Practice Pattern(®) Guidelines. *Ophthalmology*. 2016;123(1):P112-P151.
7. Weinreb RN. *Glaucoma Screening*. Kugler Publications; 2008.
8. Newman-Casey PA, Verkade AJ, Oren G, Robin AL. Gaps in Glaucoma care: A systematic review of monoscopic disc photos to screen for glaucoma. *Expert Rev Ophthalmol*. 2014;9(6):467-474.
9. Bernardes R, Serranho P, Lobo C. Digital ocular fundus imaging: a review. *Ophthalmologica*. 2011;226(4):161-181.
10. Shi L, Wu H, Dong J, Jiang K, Lu X, Shi J. Telemedicine for detecting diabetic retinopathy: a systematic review and meta-analysis. *Br J Ophthalmol*. 2015;99(6):823-831.
11. Weinreb RN, Khaw PT. Primary open-angle glaucoma. *Lancet*. 2004;363(9422):1711-1720.
12. Bowd C, Weinreb RN, Zangwill LM. Evaluating the optic disc and retinal nerve fiber layer in glaucoma. I: Clinical examination and photographic methods. *Semin Ophthalmol*. 2000;15(4):194-205.
13. Weinreb RN, Aung T, Medeiros FA. The Pathophysiology and Treatment of Glaucoma. *JAMA*. 2014;311(18):1901.
14. Prum BE Jr, Rosenberg LF, Gedde SJ, et al. Primary Open-Angle Glaucoma Preferred Practice Pattern(®) Guidelines. *Ophthalmology*. 2016;123(1):P41-P111.
15. Hollands H, Johnson D, Hollands S, Simel DL, Jinapriya D, Sharma S. Do Findings on Routine Examination Identify Patients at Risk for Primary Open-Angle Glaucoma? *JAMA*.

2013;309(19):2035.

16. Mardin CY, Horn F, Viestenz A, Lämmer R, Jünemann A. [Healthy optic discs with large cups--a diagnostic challenge in glaucoma]. *Klin Monbl Augenheilkd*. 2006;223(4):308-314.
17. Jonas JB, Fernández MC. Shape of the neuroretinal rim and position of the central retinal vessels in glaucoma. *Br J Ophthalmol*. 1994;78(2):99-102.
18. Jonas JB, Schiro D. Localized retinal nerve fiber layer defects in nonglaucomatous optic nerve atrophy. *Graefes Arch Clin Exp Ophthalmol*. 1994;32(12):759-760.
19. Chihara E, Matsuoka T, Ogura Y, Matsumura M. Retinal nerve fiber layer defect as an early manifestation of diabetic retinopathy. *Ophthalmology*. 1993;100(8):1147-1151.
20. Chaum E, Drewry RD, Ware GT, Charles S. Nerve fiber bundle visual field defect resulting from a giant peripapillary cotton-wool spot. *J Neuroophthalmol*. 2001;21(4):276-277.
21. Sutton GE, Motolko MA, Phelps CD. Baring of a circumlinear vessel in glaucoma. *Arch Ophthalmol*. 1983;101(5):739-744.
22. Fingeret M, Medeiros FA, Susanna R Jr, Weinreb RN. Five rules to evaluate the optic disc and retinal nerve fiber layer for glaucoma. *Optometry*. 2005;76(11):661-668.
23. LeCun Y, Bengio Y, Hinton G. Deep learning. *Nature*. 2015;521(7553):436-444.
24. Gulshan V, Peng L, Coram M, et al. Development and Validation of a Deep Learning Algorithm for Detection of Diabetic Retinopathy in Retinal Fundus Photographs. *JAMA*. 2016;316(22):2402-2410.
25. Krause J, Gulshan V, Rahimy E, et al. Grader Variability and the Importance of Reference Standards for Evaluating Machine Learning Models for Diabetic Retinopathy. *Ophthalmology*. 2018;125(8):1264-1272.
26. Ting DSW, Cheung CY-L, Lim G, et al. Development and Validation of a Deep Learning System for Diabetic Retinopathy and Related Eye Diseases Using Retinal Images From Multiethnic Populations With Diabetes. *JAMA*. 2017;318(22):2211-2223.
27. Sayres R, Taly A, Rahimy E, et al. Using a deep learning algorithm and integrated gradients explanation to assist grading for diabetic retinopathy. *Ophthalmology*. November 2018. doi:10.1016/j.ophtha.2018.11.016
28. Liu S, Graham SL, Schulz A, et al. A Deep Learning-Based Algorithm Identifies Glaucomatous Discs Using Monoscopic Fundus Photographs. *Ophthalmology Glaucoma*. 2018;1(1):15-22.
29. Li Z, He Y, Keel S, Meng W, Chang RT, He M. Efficacy of a Deep Learning System for Detecting Glaucomatous Optic Neuropathy Based on Color Fundus Photographs. *Ophthalmology*. 2018;125(8):1199-1206.
30. Shibata N, Tanito M, Mitsuhashi K, et al. Development of a deep residual learning algorithm

- to screen for glaucoma from fundus photography. *Sci Rep*. 2018;8(1):14665.
31. Christopher M, Belghith A, Bowd C, et al. Performance of Deep Learning Architectures and Transfer Learning for Detecting Glaucomatous Optic Neuropathy in Fundus Photographs. *Sci Rep*. 2018;8(1):16685.
 32. Thomas S-M, Jeyaraman MM, Hodge WG, Hutnik C, Costella J, Malvankar-Mehta MS. The effectiveness of teleglaucoma versus in-patient examination for glaucoma screening: a systematic review and meta-analysis. *PLoS One*. 2014;9(12):e113779.
 33. Welcome to EyePACS. <http://www.eyepacs.org>. Accessed December 5, 2018.
 34. [No title]. <http://www.inoveon.com/>. Accessed December 5, 2018.
 35. Age-Related Eye Disease Study Research Group. The Age-Related Eye Disease Study (AREDS): design implications. AREDS report no. 1. *Control Clin Trials*. 1999;20(6):573-600.
 36. Website. <http://www.ukbio-bank.ac.uk/about-biobank-uk>. Accessed December 5, 2018.
 37. Lopes FSS, Dorairaj S, Junqueira DLM, Furlanetto RL, Biteli LG, Prata TS. Analysis of neuroretinal rim distribution and vascular pattern in eyes with presumed large physiological cupping: a comparative study. *BMC Ophthalmol*. 2014;14:72.
 38. Susanna R Jr. The lamina cribrosa and visual field defects in open-angle glaucoma. *Can J Ophthalmol*. 1983;18(3):124-126.
 39. Poon LY-C, Valle DS-D, Turalba AV, et al. The ISNT Rule: How Often Does It Apply to Disc Photographs and Retinal Nerve Fiber Layer Measurements in the Normal Population? *Am J Ophthalmol*. 2017;184:19-27.
 40. Szegedy C, Vanhouke V, Ioffe S, Shlens J, Wojna Z. Rethinking the Inception Architecture for Computer Vision. *arXiv preprint arXiv:150203167*. December 2015. <http://arxiv.org/pdf/1512.00567v3.pdf>.
 41. TensorFlow - BibTex Citation. <https://chromium.googlesource.com/external/github.com/tensorflow/tensorflow/+0.6.0/tensorflow/g3doc/resources/bib.md>. Accessed December 3, 2018.
 42. Caruana R, Lawrence S, Giles L. Overfitting in Neural Nets: Backpropagation, Conjugate Gradient, and Early Stopping. In: *Advances in Neural Information Processing Systems 13: Proceedings of the 2000 Conference*. MIT Press; 2001.
 43. Krizhevsky A, Sutskever I, Hinton GE. Imagenet classification with deep convolutional neural networks. In: *Advances in Neural Information Processing Systems*. ; 2012:1097-1105.
 44. Settles B. Active Learning. *Synthesis Lectures on Artificial Intelligence and Machine Learning*. 2012;6(1):1-114.
 45. Opitz D, Maclin R. Popular Ensemble Methods: An Empirical Study. *J Artif Intell Res*.

1999;11:169-198.

46. Chihara LM, Hesterberg TC. *Mathematical Statistics with Resampling and R*; 2018.
47. Clopper CJ, Pearson ES. The Use of Confidence or Fiducial Limits Illustrated in the Case of the Binomial. *Biometrika*. 1934;26(4):404.
48. Massey FJ. The Kolmogorov-Smirnov Test for Goodness of Fit. *J Am Stat Assoc*. 1951;46(253):68.
49. Krippendorff K. *Content Analysis: An Introduction to Its Methodology*. SAGE Publications; 2018.
50. Herschler J, Osher RH. Baring of the circumlinear vessel. An early sign of optic nerve damage. *Arch Ophthalmol*. 1980;98(5):865-869.
51. Susanna R Jr, Medeiros FA. *The Optic Nerve in Glaucoma*.; 2006.
52. Tielsch JM, Katz J, Quigley HA, Miller NR, Sommer A. Intraobserver and interobserver agreement in measurement of optic disc characteristics. *Ophthalmology*. 1988;95(3):350-356.
53. Varma R, Steinmann WC, Scott IU. Expert agreement in evaluating the optic disc for glaucoma. *Ophthalmology*. 1992;99(2):215-221.